

Convolutional Pose Machines

Shih-En Wei

shihenw@cmu.edu

Varun Ramakrishna

varunnr@cs.cmu.edu

Takeo Kanade

Takeo.Kanade@cs.cmu.edu

Yaser Sheikh

yaser@cs.cmu.edu

The Robotics Institute
Carnegie Mellon University

Abstract

Pose Machines provide a powerful modular framework for articulated pose estimation. The sequential prediction framework allows for the learning of rich implicit spatial models, but currently relies on manually designed features for representing image and spatial context. In this work, we incorporate a convolutional network architecture into the pose machine framework allowing the learning of representations for both image and spatial context directly from data. The contribution of this paper is a systematic approach to composing convolutional networks with large receptive fields for pose estimation tasks. Our approach addresses the characteristic difficulty of vanishing gradients during training by providing a natural learning objective function that enforces intermediate supervision, thereby replenishing backpropagated gradients and conditioning the learning procedure. We demonstrate state-of-the-art performance and outperform competing methods on standard benchmarks including the MPII, LSP and FLIC datasets.

1. Introduction

We introduce *Convolutional Pose Machines* for the task of articulated pose estimation. Convolutional pose machines inherit the benefits of the recently proposed *pose machine* [28] architecture—the implicit learning of long-range dependencies between image, multi-scale and multi-part cues, tight integration between learning and inference, a modular sequential design—and combine them with the advantages afforded by convolutional architectures: the ability to learn feature representations for both image and spatial context directly from data; a differentiable architecture that allows for all stages to be trained jointly with backpropagation; and the ability to efficiently handle large training datasets.

Convolutional pose machines consist of a sequence of prediction networks trained to predict confidences for the locations of each part, improving their predictions in each stage of the sequence (Figure 1). When convolutional networks are composed in such a way, it results in an over-

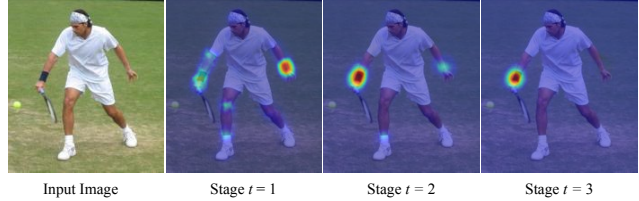


Figure 1: A **Convolutional Pose Machine** consists of a sequence of predictors trained to make a dense predictions at each image location. Here we show the increasingly refined estimates for the location of the *right wrist* in each stage of the sequence.

all network with many layers that is at risk of the problem of *vanishing gradients* [4, 5, 10, 11] during learning. This problem can occur because backpropagated gradients diminish in strength as they are propagated through the many layers of the network. While there exists recent work which shows that supervising very deep networks at intermediate layers aids in learning [19, 35], they have mostly been restricted to simpler classification problems. In this work, we show how for a *structured prediction* problem such as pose estimation, Convolutional Pose Machines naturally suggest a systematic framework that replenishes gradients by enforcing intermediate supervision periodically through the network.

The design of the network in each stage of our sequential prediction framework is motivated by the goal of achieving a large receptive field on both the image and the output predictions of the preceding stage. We find, through experiment, that large receptive fields are crucial for learning long range spatial relationships and result in improved accuracy. Large receptive fields could be achieved by different designs: increasing pooling; increasing the number of layers; or increasing the kernel size of each convolutional filter. Each of these design choices come with trade-offs in either precision of localization, increase in network depth, or increase in parameters. We discuss the design of a convolutional architecture with intermediate supervision that achieves a large receptive field allowing for the encoding of long range spatial dependencies.

Our main contributions are (a) a sequential convolutional architecture that directly learns both image and image-

dependent spatial context from data and (b) a systematic approach to composing convolutional networks with large receptive fields for pose estimation tasks without the need for any graphical model style inference. We achieve state-of-the-art results on standard benchmarks, and analyze the effects of using an architecture with intermediate supervision, providing further evidence that networks with large depths can be effectively learned via intermediate supervision.

2. Related Work

The classical approach to articulated pose estimation is the **pictorial structures** model [2, 3, 9, 13, 25, 26, 29, 42] in which spatial correlations between parts of the body are expressed as a tree-structured graphical model with kinematic priors that couple connected limbs. These methods have been successful on images where all the limbs of the person are visible, but are prone to characteristic errors such as double-counting image evidence, which occur because of correlations between variables that are not captured by a tree-structured model. The work of Kiefel et al. [16] is based on the pictorial structures model but differs in the underlying graph representation. **Hierarchical models** [34, 36] represent the relationships between parts at different scales and sizes in a hierarchical tree structure. The underlying assumption of these models is that larger parts (that correspond to full limbs instead of joints) can often have discriminative image structure that can be easier to detect and consequently help reason about the location of smaller, harder-to-detect parts. **Non-tree models** [8, 15, 18, 32, 41] incorporate interactions that introduce loops to augment the tree structure with additional edges that capture symmetry, occlusion and long-range relationships. These methods usually have to rely on approximate inference during both learning and at test time, and therefore have to trade off accurate modeling of spatial relationships with models that allow efficient inference, often with a simple parametric form to allow for fast inference. In contrast, methods based on a **sequential prediction** framework [28] learn an *implicit* spatial model with potentially complex interactions between variables by directly training an inference procedure, as in [21, 24, 30, 40].

There has been a recent surge of interest in models that employ **convolutional architectures** for the task of articulated pose estimation [6, 7, 22, 23, 27, 37, 38]. Toshev et al. [39] take the approach of directly regressing the Cartesian coordinates using a standard convolutional architecture [17]. Recent work regresses image to belief maps, and resort to graphical models, which require hand-designed energy functions or heuristic initialization of spatial probability priors, to remove outliers on the regressed belief maps. Some of them also utilize a dedicated network module for precision refinement [27, 37]. In this work, we show the regressed belief maps are suitable to be inputted to further convolutional networks with large receptive fields to learn

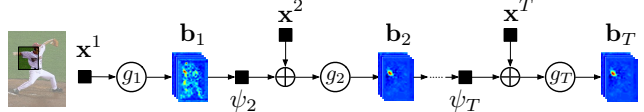


Figure 2: Pose Machines. A pose machine consists of a sequence of predictors that improve their predictions in each stage of the sequence using spatial context cues from the previous stage’s predictions.

implicit spatial dependencies without the use of hand designed priors, and achieve state-of-the-art performance over all precision region without careful initialization and dedicated precision refinement. Due to the differentiable nature of convolutions, our model can be globally trained, where Tompson et al. [38] and Steward et al. [33] also discussed the benefit of joint training.

Carreira et al. [6] train a deep network to iteratively predict error feedback, which is also in a sequential prediction framework. While they showed the benefit of predicting error instead of direct prediction, they are regressing into Cartesian errors like [39], which loses uncertainty and is difficult to learn precise mapping [38]. In this work, we show how the sequential prediction framework takes advantage of the preserved uncertainty in the belief maps to encode the rich spatial context, with enforcing the intermediate local supervisions to address the problem of vanishing gradients.

3. Method

3.1. Pose Machines

We denote the pixel location of the p -th anatomical landmark (which we refer to as a part), $Y_p \in \mathcal{Z} \subset \mathbb{R}^2$, where \mathcal{Z} is the set of all (u, v) locations in an image. Our goal is to predict the image locations $Y = (Y_1, \dots, Y_P)$ for all P parts. A pose machine [28] (see Figure 2) consists of a sequence of multi-class predictors, $g_t(\cdot)$, that are trained to predict the location of each part in each level of the hierarchy. In each *stage* $t \in \{1 \dots T\}$, the classifiers g_t predict confidences for assigning a location to each part $Y_p = z$, $\forall z \in \mathcal{Z}$, based on features extracted from the image at the location z denoted by $\mathbf{x}_z^t \in \mathbb{R}^d$ and contextual information from the preceding classifier in the neighborhood around each Y_p in stage t . A classifier in the first stage $t = 1$, therefore produces the following confidence values:

$$g_1(\mathbf{x}_z^1) \rightarrow \{b_1^p(Y_p = z)\}_{p \in \{0 \dots P\}}, \quad (1)$$

where $b_1^p(Y_p = z)$ is the score predicted by the classifier g_1 for assigning the p^{th} part in the first stage at image location z . We represent all the confidences, or *beliefs*, of part p evaluated at every location $z = (u, v)^T$ in the image as $\mathbf{b}_t^p \in \mathbb{R}^{w \times h}$, where w and h are the width and height of the image, respectively. That is,

$$\mathbf{b}_t^p[u, v] = b_t^p(Y_p = z). \quad (2)$$

For convenience, we denote the collection of confidence maps for all the parts as $\mathbf{b}_t \in \mathbb{R}^{w \times h \times (P+1)}$.

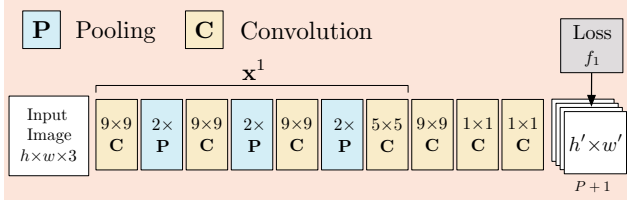


Figure 3: Convolutional Architecture for Keypoint Localization. A deep convolutional architecture for performing keypoint localization that relies on local image evidence in a small region (receptive field) around each pixel location.

In subsequent stages, the classifier predicts a confidence for assigning a location to each part $Y_p = z$, $\forall z \in \mathcal{Z}$, based on (1) features of the image data $\mathbf{x}_z^t \in \mathbb{R}^d$ again, and (2) contextual information from the preceding classifier in the neighborhood around each Y_p :

$$g_t(\mathbf{x}_z^t, \psi_t(z, \mathbf{b}_{t-1})) \rightarrow \{b_t^p(Y_p = z)\}_{p \in \{0 \dots P\}}, \quad (3)$$

where $\psi_{t>1}(\cdot)$ is a mapping from the confidences \mathbf{b}_{t-1} to context features. In each stage, the computed confidences provide an increasingly refined estimate for the location of each part. Note that, to be more general, we allow image features \mathbf{x}_z^t for each stage can be different here, while in practice they can be shared across stages. The pose machine proposed in [28] used boosted random forests for prediction ($\{g_t\}$), fixed hand-crafted image features across all stages (\mathbf{x}_z^t), and context feature maps ($\psi_t(\cdot)$) to capture spatial context across all stages.

3.2. Convolutional Pose Machines

We show how the prediction and image feature computation modules of a pose machine can be replaced by a deep convolutional architecture allowing for both image and contextual feature representations to be learned directly from data. Convolutional architectures also have the advantage of being completely differentiable, thereby enabling end-to-end joint training of all stages of a pose machine. We describe our design for a Convolutional Pose Machine that combines the advantages of deep convolutional architectures with the implicit spatial modeling afforded by the pose machine framework.

3.2.1 Keypoint Localization Using Local Image Evidence

The first stage of a convolutional pose machine predicts part confidences from only local image evidence. Figure 3 shows the network structure used for part detection from local image evidence using a deep convolutional network. The evidence is *local* because the receptive field of the first stage of the network is constrained to a cropped small patch around the keypoint location. We use a network structure composed of five convolutional layers followed by two 1×1 convolutional layers which results in a fully convolutional architecture [20] (see Figure 3). In practice, to

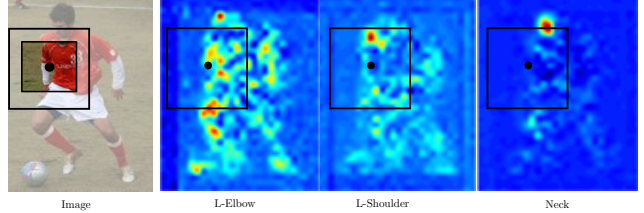


Figure 4: Spatial context from confidence maps can provide valuable cues for detection. The peaks in the confidence map for easier to detect landmarks, such as the shoulder, can be a strong cue for the location of difficult to detect landmarks, such as the left elbow.

achieve certain precision, we input normalized images of size 368×368 , and the receptive field of the network shown above is 160×160 pixels. The network can effectively be viewed as sliding a deep network across an image and regressing from the local image evidence in each 160×160 image patch to a $P+1$ (plus one for background) sized output vector that represents a score for each part at that image location.

3.2.2 Sequential Prediction with Learned Spatial Context Features

While the detection rate on landmarks with consistent appearance, such as the head and shoulders, can be favorable, the accuracies are often much lower for landmarks lower down the kinematic chain of the human skeleton due to their large variance in configuration and appearance. The landscape of the confidence maps around a part location, albeit noisy, can, however, be very informative. The fact that the confidence map for the shoulder has a sharp peak in the vicinity of the shoulder can be used as a strong cue for predicting the location of the elbow (see Figure 4). A predictor in subsequent stages ($g_{t>1}$) can use the spatial context ($\psi_{t>1}(\cdot)$) of the noisy confidence maps in a region around the image location z and improve its predictions by leveraging the fact that parts occur in consistent geometric configurations. In the second stage of a pose machine, the classifier g_2 accepts as input the image features \mathbf{x}_z^2 and features computed on the confidences via the feature function ψ for each of the parts in the previous stage. The feature function ψ serves to encode the landscape of the confidence maps from the previous stage in a spatial region around the location z of the different parts. For a convolutional pose machine, we do not have an explicit function that computes context features. Instead, we define ψ as being the receptive field of the predictor on the confidences from the previous stage.

The design of the network is guided by achieving a receptive field at the output layer of the second stage network that is large enough to allow the learning of potentially complex and long-range correlations between parts. By simply supplying features on the outputs of the previous stage (as opposed to specifying potential functions in a graphical model), the convolutional layers in the subsequent stage allow the classifier to freely combine contextual informa-

Convolutional Architecture for a 2-Stage Pose Machine

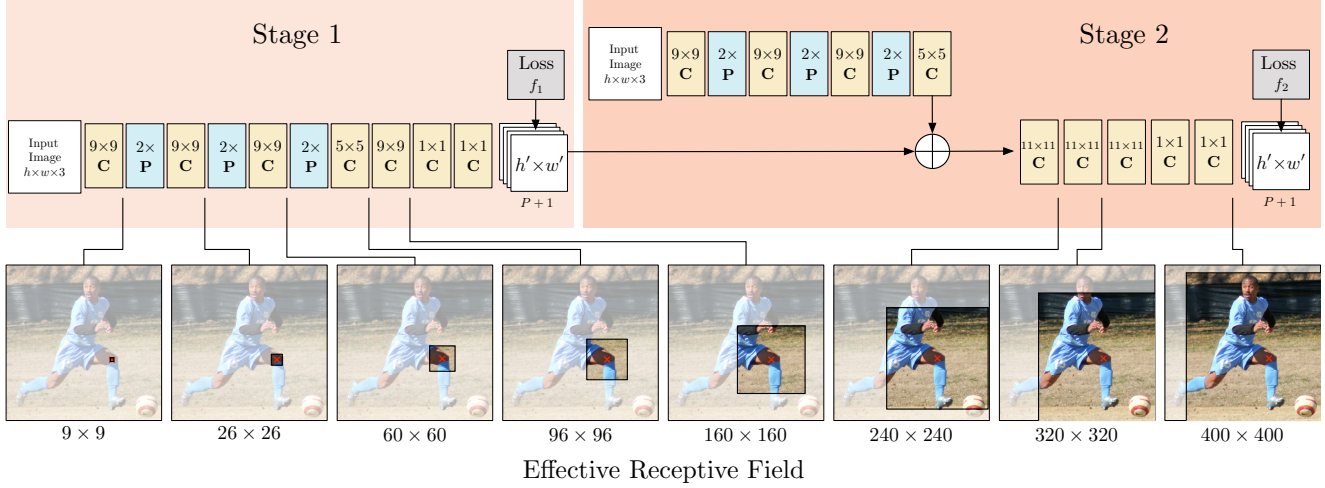


Figure 5: Receptive Field of a 2-stage Pose Machine. We show a deep convolutional architecture and receptive fields across layers for a pose machine with two stages. In the second stage we use a convolutional architecture that uses both confidence maps from the previous stage as well as features learned directly from the image. Below, we show the effective receptive field on an image (centered at left knee) of the architecture. Note the achieved large receptive enables the model to capture long-range spatial dependencies such as those between the head and the knees.

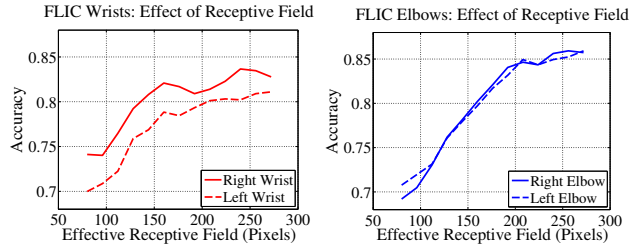


Figure 6: Large receptive fields for spatial context. We show that networks with large receptive fields are effective at modeling long range spatial interactions between parts. Note the experiments are operated with smaller normalized images than our best setting.

tion by picking the most predictive features. The confidence maps from the first stage are generated from a network that examined the image locally with a small receptive field. In the second stage, we design a network that drastically increases the equivalent receptive field. Large receptive fields can be achieved either by pooling at the expense of precision, increasing the kernel size of the convolutional filters at the expense of increasing the number of parameters, or by increasing the number of convolutional layers at the risk of encountering vanishing gradients during training. Our design for the two stage network is shown in Figure 5. We choose to use multiple convolutional layers to achieve large receptive field on the $8 \times$ downscaled heatmaps, as it allows us to be parsimonious with respect to the number of parameters of the model. We found that our stride-8 network performs as well as a stride-4 one even at high precision region, while it makes us easier to achieve larger receptive fields. We also repeat similar structure for image feature maps to make the spatial context be image-dependent and allow error correction, following the structure of pose machine.

We find that accuracy improves with the size of the receptive field. In Figure 6 we show the improvement in accuracy on the FLIC dataset [31] as the size of the receptive field on the original image is varied by varying the architecture without significant change on number of parameters, through a series of experimental trials on input images normalized to a size of 304×304 . We see that the accuracy improves as the effective receptive field increases, and starts to saturate around 250 pixels, which also happens to be roughly the size of the normalized object. This improvement in accuracy with receptive field size suggests that the network does indeed encode long range interactions between parts and that doing so is beneficial. In our best performing setting in Figure 5, we normalized images into a larger size of 368×368 pixels for better precision, and the receptive field of the second stage output on the confidence maps of the first stage is set to 31×31 , which is equivalently 400×400 pixels on the original image, where the radius can usually cover from any two of the parts. With more stages, the effective receptive field is even larger. In the following section we show our results from up to 6 stages.

3.3. Learning in Convolutional Pose Machines

The design described above for a pose machine results in a deep architecture that can have a large number of layers. Training such a network with many layers can be prone to the problem of *vanishing gradients* [4, 5, 10] where, as observed by Bradley [5] and Bengio et al. [10], the magnitude of back-propagated gradients decreases in strength with the number of intermediate layers between the output layer and the input layer.

Fortunately, the sequential prediction framework of the pose machine provides a natural approach to training our deep architecture that addresses this problem. Each stage of

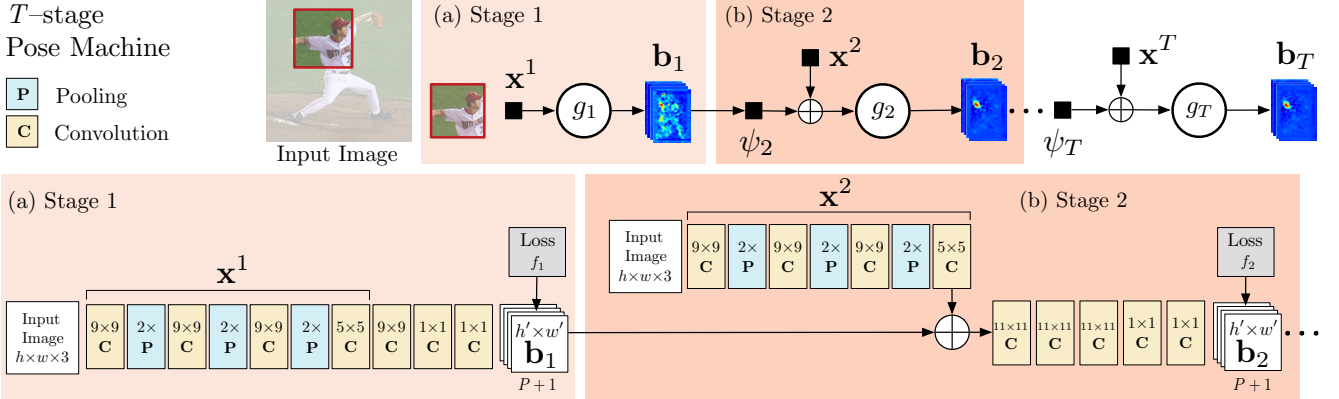


Figure 7: Architecture for a T -stage Convolutional Pose Machines. We show a deep convolutional architecture for a pose machine with any number stages. The pose machine is shown in the top right with insets described below. Insets (a) shows the architecture that operates only on image evidence in the first stage. Insets (b) shows the architecture for subsequent stages, which operate both on image evidence as well as confidence maps from preceding stages. The architectures in (b) is repeated for all subsequent stages (2 to T). The network is locally supervised after each stage using an intermediate loss layer that prevents vanishing gradients during training. (Best viewed in color.)

the pose machine is trained to repeatedly produce the confidence maps or *beliefs* for the locations of each of the parts. We encourage the network to repeatedly arrive at such a representation by defining a loss function at the output of each stage t that minimizes the l_2 distance between the predicted and ideal confidence maps for each part. The ideal confidence map for a part p is written as $b_*^p (Y_p = z)$, which are created by putting Gaussian peaks at ground truth locations of each body part p . The cost function we aim to minimize at the output of each stage at each level is therefore given by:

$$f_t = \sum_{p=1}^{P+1} \sum_{z \in \mathcal{Z}} \|b_t^p(z) - b_*^p(z)\|_2^2. \quad (4)$$

The overall objective for the full architecture is obtained by adding the losses at each stage and is given by:

$$\mathcal{F} = \sum_{t=1}^T f_t. \quad (5)$$

We use standard stochastic gradient descend to jointly train all the T stages in the network. To make the training efficient, we share the weights of convolutional layers for image features (corresponding to $\mathbf{x}^2, \mathbf{x}^3, \dots, \mathbf{x}^T$) across all the subsequent stages.

4. Evaluation

4.1. Analysis

Addressing vanishing gradients. The objective in Equation 5 describes a decomposable loss function that operates on different parts of the network (see Figure 7). Specifically, each term in the summation is applied to the network after each stage t effectively enforcing supervision in intermediate stages through the network. Intermediate supervision has the advantage that, even though the full architecture can

have many layers, it does not fall prey to the *vanishing gradient* problem as the intermediate loss functions replenish the gradients at each stage.

We verify this claim by observing histograms of gradient magnitude (see Figure 9) at different depths in the architecture across training epochs for models with and without intermediate supervision. In early epochs, as we move from the output layer to the input layer, we observe on the model *without intermediate supervision*, the gradient distribution is tightly peaked around zero because of vanishing gradients. The model *with intermediate supervision* has a much larger variance across all the layers, suggesting that learning is indeed occurring in all the layers thanks to intermediate supervision. We also notice that as training progresses, the variance in the gradient magnitude distributions decreases pointing to model convergence.

Benefit of end-to-end learning. We see in Figure 8a that replacing the modules of a pose machine with the appropriately designed convolutional architecture provides a large boost of 42.4 percentage points over the previous approach of [28] in the high precision regime (PCK@0.1) and 30.9 percentage points in the low precision regime (PCK@0.2).

Which learning method? We compare different variants of training the network in Figure 8b on the LSP dataset with person-centric (PC) annotation and demonstrate the benefit of intermediate supervision with joint training across stages using a model trained in four ways: (i) training from scratch using a global loss function that enforces intermediate supervision (ii) stage-wise; where each stage is trained in a feed-forward fashion and stacked (iii) as same as (i) but initialized with weights from (ii), and (iv) as same as (i) but with no intermediate supervision. We find that network (i) outperforms all other training methods, showing that intermediate supervision and joint training across stage is indeed crucial in achieving good performance. The stagewise training in (ii) saturate at sub-optimal very soon and the jointly finetuning (iii) improves from this sub-optimal to the ac-

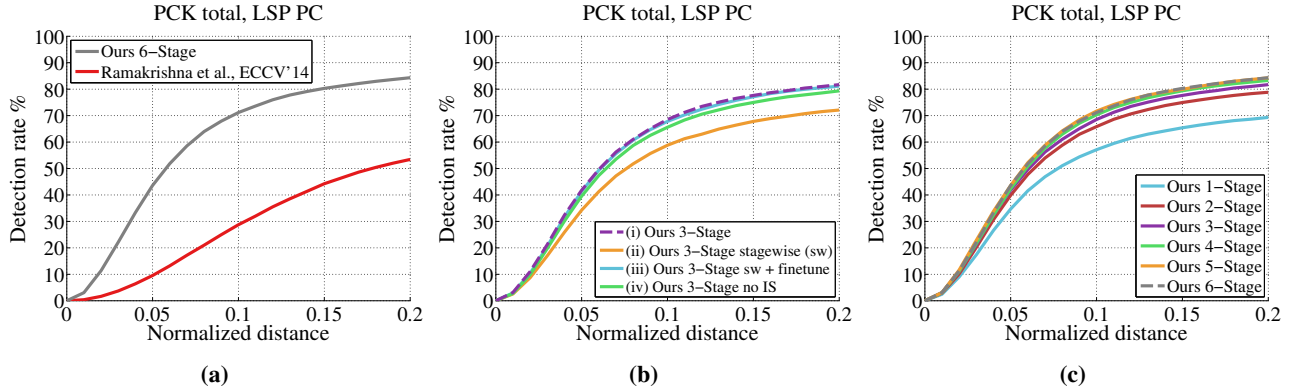


Figure 8: Comparisons on 3-stage architectures on the LSP dataset (PC): (a) Improvements over Pose Machine. (b) Comparisons between the different training methods. (c) Comparisons across each number of stages using joint training from scratch with intermediate supervision.

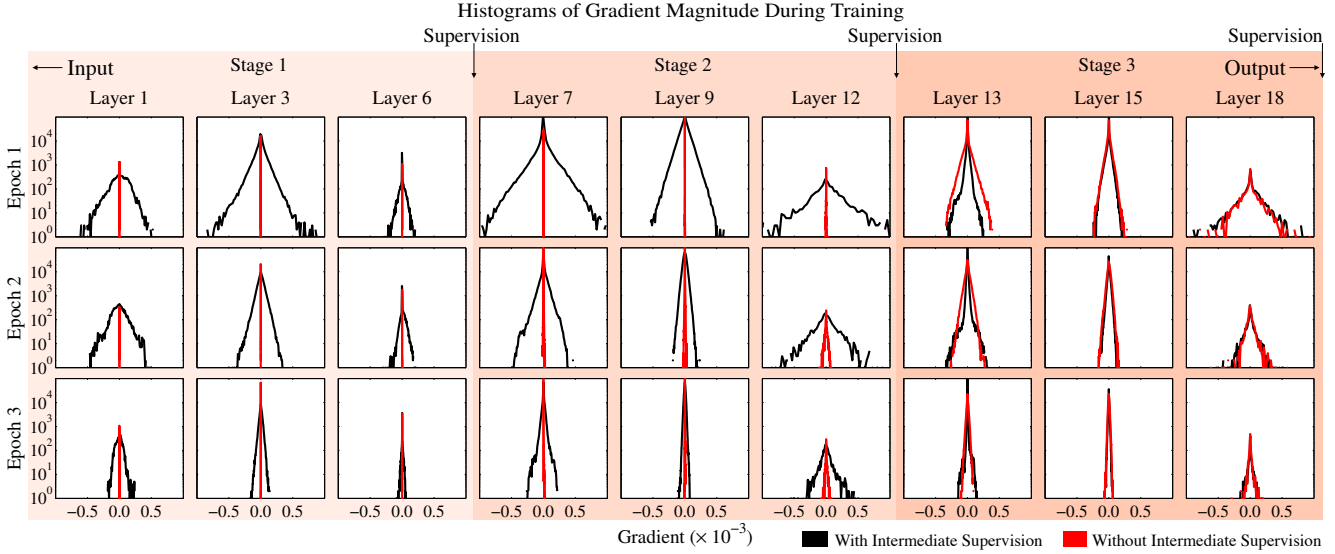


Figure 9: Intermediate supervision addresses vanishing gradients. We track the change in magnitude of weights in layers at different depths in the network, across training epochs, for models with and without intermediate supervision. We observe that for layers closer to the output the distribution has a large variance for both with and without intermediate supervision, however as we move from the output layer towards the input, the gradient magnitude distribution peaks tightly around zero with low variance (the gradients *vanish*) for the model without intermediate supervision. For the model with intermediate supervision the distribution has a moderately large variance throughout the network. At later training epochs, the variances decrease for all layers for the model with intermediate supervision and remain tightly peaked around zero for the model without intermediate supervision. (Best viewed in color)

curacy level closed to (i), however with effectively longer training iterations.

Performance across stages. We show a comparison of performance across each stage on the LSP dataset (PC) in Figure 8c. We show that the performance increases monotonically until 5 stages, as the predictors in subsequent stages make use of contextual information in a large receptive field on the previous stage confidence maps to resolve confusions between parts and background. We see diminishing returns at the 6th stage, which is the number we choose for reporting our best results in this paper for LSP and MPI dataset.

4.2. Datasets and Quantitative Analysis

We define and implement our model using the *Caffe* [12] libraries for deep learning. We publicly release the source code and details on the architecture, learning parameters,

design decisions and data augmentation to ensure full reproducibility.¹

MPII Human Pose Dataset. We show in Figure 12 our results on the MPII Human Pose dataset [1] which consists more than 28000 training samples. We choose to randomly augment the data with rotation degrees in $[-40^\circ, 40^\circ]$, scaling with factors in $[0.7, 1.3]$, and horizontal flipping. The evaluation is based on PCKh metric [1] where the error tolerance is normalized with respect to head size of the target. Because there often are multiple people in the proximity of the interested person (rough center position is given in the dataset), we made two sets of ideal heatmaps for training: one is including all the peaks for every people appearing in the proximity, and the other one only contains peaks of

¹<http://github.com/shihenw/convolutional-pose-machines-release>

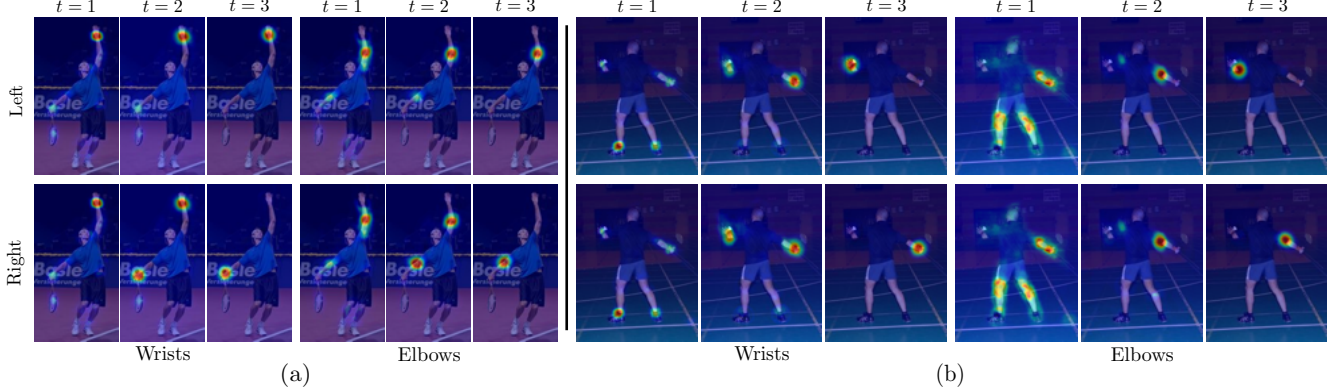


Figure 10: Comparison of confidence maps across stages for the elbow and wrist joints on the LSP dataset for a three stage deep pose machine. The subsequent stages of the convolutional pose machine learn a spatial model that aids in resolving confusions between parts. The first stage predictions for the wrist joints are often ambiguous or erroneous.

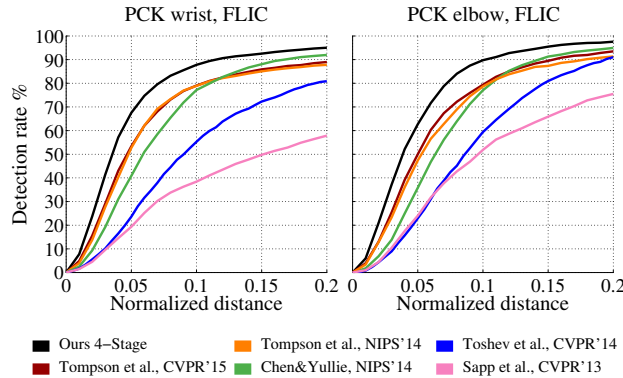


Figure 11: Quantitative results for the elbow and wrist joints on the FLIC dataset for a convolutional pose machine with 4 stages. We outperform all competing methods.

the interested person. We feed the first set of heatmap into the loss layer of the first stage, to make the first stage concentrate on recognizing local parts, and feed the second set of heatmap into all the subsequent loss layers. With an extra heatmap channel with a single Gaussian peak (of larger variance) indicating the center of interested person cascaded (at the ‘‘cascading point’’ of each subsequent stage), the following stages can use this clue to suppress those responses fired on surrounding people.

Our total PCKh-0.5 score achieves state of the art at 87.95% (88.52% with adding LSP data), which is 6.11% higher than the closest competitor, and it is noteworthy that on the ankle (the most challenging part), our PCKh-0.5 score is 78.28% (79.41% with adding LSP data), which is 10.76% higher than the closest competitor. This result shows the capability of our model to capture long distance context given ankles are the farthest parts from head and other more recognizable parts. Our method improves the accuracy in all parts and over all precisions, and is the first one achieving such high accuracy without any pre-training from other data, or post-inference parsing with hand-design priors or initialization of such a structured prediction task as

in [27, 38]. Our methods also does not need another module dedicated to location refinement as in [37] to achieve good high-precision accuracy with a stride-8 network.

Leeds Sports Pose (LSP) Dataset. We evaluate our method on the Extended Leeds Sports Dataset [14] that consists of 11000 images for training and 1000 images for testing. We trained on person-centric (PC) annotations and evaluate our method using the Percentage Correct Keypoints (PCK) metric [43]. Using the same augmentation scheme as for the MPI dataset, our model again achieves state of the art at 84.32% (90.5% with adding MPI data). Note that adding MPI data here significantly boosts our performance, due to its labeling quality is much better than LSP. Because of the noisy label in the LSP dataset, Pishchulin et al. [27] relabeled them for their method.

FLIC Dataset. We evaluate our method on the FLIC Dataset [31] which consists of 3987 images for training and 1016 images for testing. We report accuracy as per the metric introduced in Sapp et al. [31] for the elbow and wrist joints in Figure 11. Again, we outperform all prior art at PCK@0.2 with 97.59% on elbows and 95.03% on wrists. In higher precision region our advantage is even more significant: 14.8 percentage points on wrists and 12.7 percentage points on elbows at PCK@0.05, and 8.9 percentage points on wrists and 9.3 percentage points on elbows at PCK@0.1.

5. Discussion

The sequential prediction framework of pose machines provides a systematic framework to compose deep architectures for pose estimation. The training procedure describes a natural objective for learning a deep architecture with many layers by enforcing intermediate supervision addressing the *vanishing gradient* problem. Some failure cases include examples with rare poses, multiple people in close proximity and heavy occlusions. The model allows for making dense predictions that leverage semantic spatial context and future work would explore application in problem domains such as jointly person detection and depth prediction.

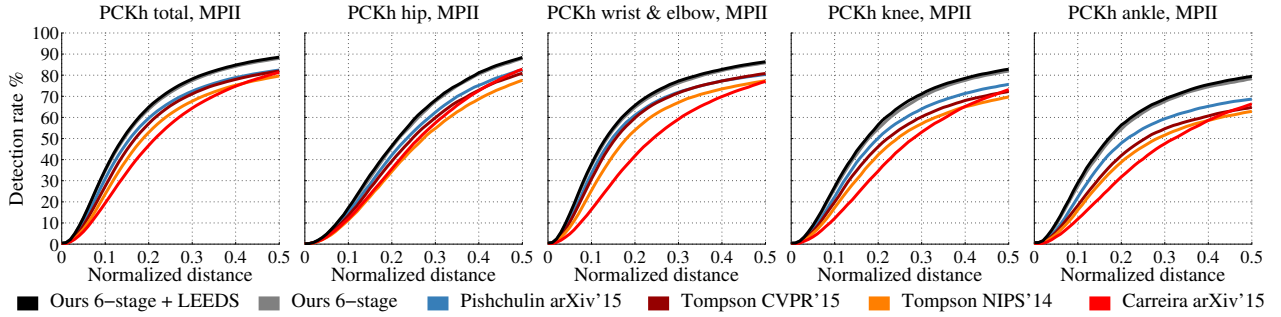


Figure 12: Quantitative results on the MPII dataset using the PCKh metric. We achieve state of the art performance and outperform significantly on difficult parts such as the ankle.

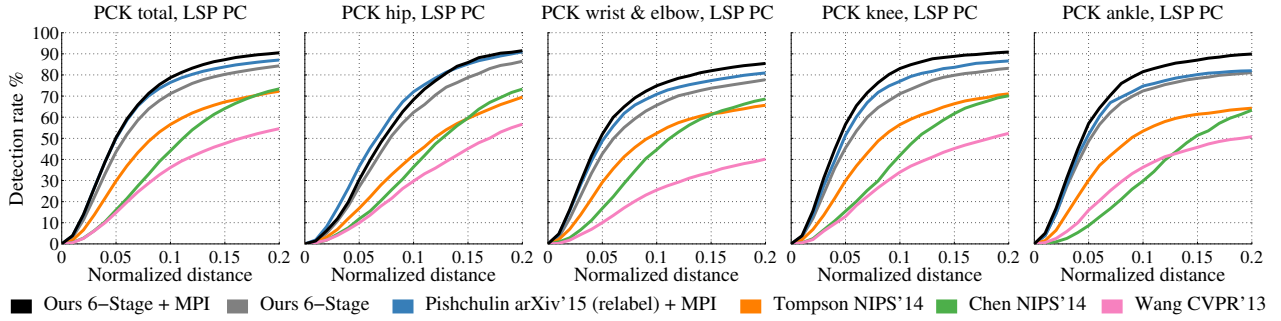


Figure 13: Quantitative results on the LSP dataset using the PCK metric. Our method again achieves state of the art performance and has a significant advantage on challenging parts.

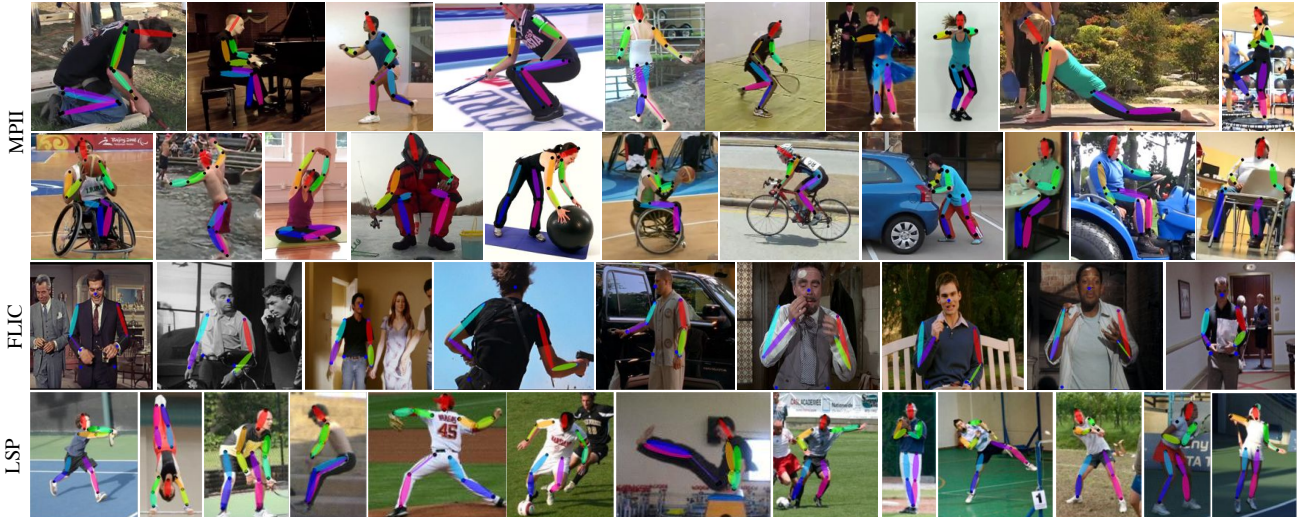


Figure 14: Qualitative results of our method on the MPII, LSP and FLIC datasets respectively. We see that the method is able to handle non-standard poses and resolve ambiguities between symmetric parts for a variety of different relative camera views.

References

- [1] M. Andriluka, L. Pishchulin, P. Gehler, and B. Schiele. 2D human pose estimation: New benchmark and state of the art analysis. In *CVPR*, 2014. [6](#)
- [2] M. Andriluka, S. Roth, and B. Schiele. Pictorial structures revisited: People detection and articulated pose estimation. In *CVPR*, 2009. [2](#)
- [3] M. Andriluka, S. Roth, and B. Schiele. Monocular 3D pose estimation and tracking by detection. In *CVPR*, 2010. [2](#)
- [4] Y. Bengio, P. Simard, and P. Frasconi. Learning long-term dependencies with gradient descent is difficult. *IEEE Transactions on Neural Networks*, 1994. [1, 4](#)
- [5] D. Bradley. *Learning In Modular Systems*. PhD thesis, Robotics Institute, Carnegie Mellon University, Pittsburgh, PA, 2010. [1, 4](#)
- [6] J. Carreira, P. Agrawal, K. Fragiadaki, and J. Malik. Human pose estimation with iterative error feedback. *arXiv preprint arXiv:1507.06550*, 2015. [2](#)
- [7] X. Chen and A. Yuille. Articulated pose estimation by a

graphical model with image dependent pairwise relations. In *NIPS*, 2014. 2

[8] M. Dantone, J. Gall, C. Leistner, and L. Van Gool. Human pose estimation using body parts dependent joint regressors. In *CVPR*, 2013. 2

[9] P. Felzenszwalb and D. Huttenlocher. Pictorial structures for object recognition. In *IJCV*, 2005. 2

[10] X. Glorot and Y. Bengio. Understanding the difficulty of training deep feedforward neural networks. In *AISTATS*, 2010. 1, 4

[11] S. Hochreiter, Y. Bengio, P. Frasconi, and J. Schmidhuber. Gradient flow in recurrent nets: the difficulty of learning long-term dependencies. *A Field Guide to Dynamical Recurrent Neural Networks*, IEEE Press, 2001. 1

[12] Y. Jia, E. Shelhamer, J. Donahue, S. Karayev, J. Long, R. Girshick, S. Guadarrama, and T. Darrell. Caffe: Convolutional architecture for fast feature embedding. *arXiv preprint arXiv:1408.5093*, 2014. 6

[13] S. Johnson and M. Everingham. Clustered pose and non-linear appearance models for human pose estimation. In *BMVC*, 2010. 2

[14] S. Johnson and M. Everingham. Learning effective human pose estimation from inaccurate annotation. In *CVPR*, 2011. 7

[15] L. Karlinsky and S. Ullman. Using linking features in learning non-parametric part models. In *ECCV*, 2012. 2

[16] M. Kiefel and P. V. Gehler. Human pose estimation with fields of parts. In *ECCV*, 2014. 2

[17] A. Krizhevsky, I. Sutskever, and G. E. Hinton. Imagenet classification with deep convolutional neural networks. In *NIPS*, 2012. 2

[18] X. Lan and D. Huttenlocher. Beyond trees: Common-factor models for 2D human pose recovery. In *ICCV*, 2005. 2

[19] C.-Y. Lee, S. Xie, P. Gallagher, Z. Zhang, and Z. Tu. Deeply-supervised nets. In *AISTATS*, 2015. 1

[20] J. Long, E. Shelhamer, and T. Darrell. Fully convolutional networks for semantic segmentation. In *CVPR*, 2015. 3

[21] D. Munoz, J. Bagnell, and M. Hebert. Stacked hierarchical labeling. In *ECCV*, 2010. 2

[22] W. Ouyang, X. Chu, and X. Wang. Multi-source deep learning for human pose estimation. In *CVPR*, 2014. 2

[23] T. Pfister, J. Charles, and A. Zisserman. Flowing convnets for human pose estimation in videos. In *ICCV*, 2015. 2

[24] P. Pinheiro and R. Collobert. Recurrent convolutional neural networks for scene labeling. In *ICML*, 2014. 2

[25] L. Pishchulin, M. Andriluka, P. Gehler, and B. Schiele. Poselet conditioned pictorial structures. In *CVPR*, 2013. 2

[26] L. Pishchulin, M. Andriluka, P. Gehler, and B. Schiele. Strong appearance and expressive spatial models for human pose estimation. In *ICCV*, 2013. 2

[27] L. Pishchulin, E. Insafutdinov, S. Tang, B. Andres, M. Andriluka, P. Gehler, and B. Schiele. Deepcut: Joint subset partition and labeling for multi person pose estimation. *arXiv preprint arXiv:1511.06645*, 2015. 2, 7

[28] V. Ramakrishna, D. Munoz, M. Hebert, J. Bagnell, and Y. Sheikh. Pose Machines: Articulated Pose Estimation via Inference Machines. In *ECCV*, 2014. 1, 2, 3, 5

[29] D. Ramanan, D. A. Forsyth, and A. Zisserman. Strike a Pose: Tracking people by finding stylized poses. In *CVPR*, 2005. 2

[30] S. Ross, D. Munoz, M. Hebert, and J. Bagnell. Learning message-passing inference machines for structured prediction. In *CVPR*, 2011. 2

[31] B. Sapp and B. Taskar. MODEC: Multimodal Decomposable Models for Human Pose Estimation. In *CVPR*, 2013. 4, 7

[32] L. Sigal and M. Black. Measure locally, reason globally: Occlusion-sensitive articulated pose estimation. In *CVPR*, 2006. 2

[33] R. Stewart and M. Andriluka. End-to-end people detection in crowded scenes. *arXiv preprint arXiv:1506.04878*, 2015. 2

[34] M. Sun and S. Savarese. Articulated part-based model for joint object detection and pose estimation. In *ICCV*, 2011. 2

[35] C. Szegedy, W. Liu, Y. Jia, P. Sermanet, S. Reed, D. Anguelov, D. Erhan, V. Vanhoucke, and A. Rabinovich. Going deeper with convolutions. *arXiv preprint arXiv:1409.4842*, 2014. 1

[36] Y. Tian, C. L. Zitnick, and S. G. Narasimhan. Exploring the spatial hierarchy of mixture models for human pose estimation. In *ECCV*, 2012. 2

[37] J. Tompson, R. Goroshin, A. Jain, Y. LeCun, and C. Bregler. Efficient object localization using convolutional networks. In *CVPR*, 2015. 2, 7

[38] J. Tompson, A. Jain, Y. LeCun, and C. Bregler. Joint training of a convolutional network and a graphical model for human pose estimation. In *NIPS*, 2014. 2, 7

[39] A. Toshev and C. Szegedy. DeepPose: Human pose estimation via deep neural networks. In *CVPR*, 2013. 2

[40] Z. Tu and X. Bai. Auto-context and its application to high-level vision tasks and 3d brain image segmentation. In *TPAMI*, 2010. 2

[41] Y. Wang and G. Mori. Multiple tree models for occlusion and spatial constraints in human pose estimation. In *ECCV*, 2008. 2

[42] Y. Yang and D. Ramanan. Articulated pose estimation with flexible mixtures-of-parts. In *CVPR*, 2011. 2

[43] Y. Yang and D. Ramanan. Articulated human detection with flexible mixtures of parts. In *TPAMI*, 2013. 7